Wave Generation in 3D Numerical Wave Tanks

by Makoto Arai*, *Member* Uttam Kumer Paul**, *Member*
Yoshiyuki Inoue*, *Member*

Summary

First and second order finite difference approximations are used in the simulations of this study to generate progressive waves in a three dimensional numerical wave tank. Some segmented numerical wave makers are set at the left end of the tank which is considered as the wave generating end. Waves propagating at different angles with longitudinal axis are generated at this end and sent towards the right end of the tank which is treated as an open boundary. A velocity reduction technique is applied to reduce the vertical velocity within a zone named Velocity Reduction Zone (VRZ) adjacent to the open boundary. In order to control the fluid motion at the open boundary, Sommerfeld Radiation Condition (SRC) is applied on that reduced waves. The generated waves with first and second order computations are compared and the superiority of the second order approximations is discussed. An example of three dimensional wave generation is also presented in this paper.

1. Introduction

Wave related problems of marine structures play important roles in the field of Naval Architecture and Ocean Engineering. Investigations of these kinds of problems require numerous model testing experiments which are not only very costly but also time consuming. But nowadays, with the advent of high speed computers, we can reach very close to the practical model testing systems of physical laboratories with the help of numerical computing systems. The introduction of more and more advanced high capacity computer systems have made us able to implement some computational methods which were once beyond our capacity. Development and use of numerical wave tanks is, therefore, one of the promising ideas in the field of fluid dynamics, where free surface problems like numerical wave generation and its propagation cover a wide range of applications.

To develop a useful numerical wave tank, special attentions have to be given on some important aspects, such as: wave generating system, open boundary treatment, free surface treatment etc. Recently many researchers are applying different procedures for numerical wave generation. She et al[1] generated monochromatic waves using a paddle moving with an angular speed given by a cosine function. A similar procedure with piston type wave maker was used by Hinatsu[2]. Ohyama et al[3] used a wave generator composed of a series of vertically aligned point sources in the computational domain. Park et al[4] applied two different computational methods for numerical wave generation and discussed on the accuracy of numerical wave making techniques. In our study, we have applied some functions for velocity components and wave elevation at the inflow boundary of the computational domain to generate waves numerically.

The next important and probably the most difficult part of this kind of study is the treatment of open boundary. Many researchers tried to treat open boundary in numerical computations applying different methods. In our previous paper[5] we have briefly discussed several researchers' procedures of open boundary treatments and we proposed a new technique for the treatment of open boundary in numerical wave tanks. The same method is also applied in this study for open boundary treatment, which consists of a velocity reduction technique and application of Sommerfeld radiation condition (SRC).

First and second order finite difference approximations are used in the numerical simulations of this study to generate progressive waves in a three dimensional wave tank. Some segmented numerical wave makers are set at the inflow boundary of the tank which is considered as the wave generating end. Two dimensional waves propagating along the longitudinal axis and oblique waves, that is, waves propagating at different angles with longitudinal axis are generated at

* Faculty of Engineering, Yokohama National University
** Graduate School, Yokohama National University

Received 9th July 1993
Read at the Autumn meeting 9, 10th Nov. 1993

this end and sent towards the right end of the tank which is considered as the open or radiation boundary. A velocity reduction technique is applied to reduce the vertical velocity within a zone called velocity reduction zone (VRZ) adjacent to the open boundary. In order to radiate the waves through the open boundary and to control the fluid motion there, Sommerfeld radiation condition (SRC) is applied on that reduced waves.

Three different sizes of the meshes are used in both first and second order computations. The results obtained from these two methods are compared with each other which shows the superiority of the second order approximations over the first order method.

2. Mathematical Formulation

2.1 Governing equations

The governing equations for a three dimensional incompressible and inviscid fluid flow in terms of Cartesian co-ordinates (x, y, z) are:

The mass continuity equation,

$$\frac{\partial u}{\partial x}+\frac{\partial v}{\partial y}+\frac{\partial w}{\partial z}=0 \tag{1}$$

and the Euler's equations of motion,

$$\frac{\partial u}{\partial t}+u\frac{\partial u}{\partial x}+v\frac{\partial u}{\partial y}+w\frac{\partial u}{\partial z}=-\frac{\partial p}{\rho\partial x} \tag{2}$$

$$\frac{\partial v}{\partial t}+u\frac{\partial v}{\partial x}+v\frac{\partial v}{\partial y}+w\frac{\partial v}{\partial z}=-\frac{\partial p}{\rho\partial y} \tag{3}$$

$$\frac{\partial w}{\partial t}+u\frac{\partial w}{\partial x}+v\frac{\partial w}{\partial y}+w\frac{\partial w}{\partial z}=-\frac{\partial p}{\rho\partial z}+g \tag{4}$$

where,

u : velocity component in x-direction,
v : velocity component in y-direction,
w : velocity component in z-direction,
ρ : density of water,
p : pressure,
g : acceleration due to gravity.

2.2 Finite difference expressions

The finite difference approximations of the governing equations are made on the basis of a staggered mesh system with constant grid spacings Δx, Δy, Δz in longi tudinal, lateral and vertical directions respectively. Fig. 1 shows a typical three dimensional finite difference cell (i, j, k). The evaluating positions of the velocity components u, v and w are shown at the centers of three faces and pressure p is located at the center of the cell. The superscript n used in the finite difference expressions designates time instant $t(t=n\cdot\Delta t$, where, Δt is time increment) at which the quantities are evaluated.

The first order finite difference approximation of the continuity equation is written as

$$\frac{(u^{n+1}_{i+\frac{1}{2},j,k}-u^{n+1}_{i-\frac{1}{2},j,k})}{\Delta x}+\frac{v^{n+1}_{i,j+\frac{1}{2},k}-v^{n+1}_{i,j-\frac{1}{2},k})}{\Delta y}+\frac{(w^{n+1}_{i,j,k+\frac{1}{2}}-w^{n+1}_{i,j,k-\frac{1}{2}})}{\Delta z}=0 \tag{5}$$

and the equations of motion are approximated as conservative forms by

$$u^{n+1}_{i+\frac{1}{2},j,k}=u^{n}_{i+\frac{1}{2},j,k}+\Delta t\left\{\frac{1}{\rho\Delta x}(p^{n}_{i,j,k}-p^{n}_{i+1,j,k})-\left[\frac{\partial u^2}{\partial x}\right]^{n}_{i+\frac{1}{2},j,k}-\left[\frac{\partial uv}{\partial y}\right]^{n}_{i+\frac{1}{2},j,k}-\left[\frac{\partial uw}{\partial z}\right]^{n}_{i+\frac{1}{2},j,k}\right\} \tag{6}$$

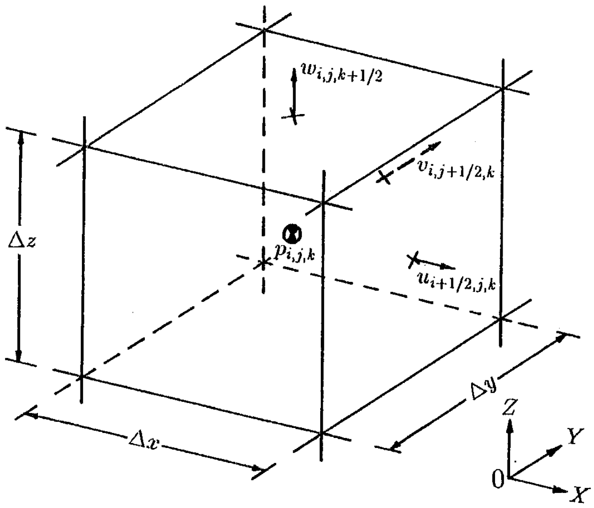

Fig. 1 Positions of the variables in a typical finite difference cell (i, j, k)

$$v^{n+1}_{i,j+\frac{1}{2},k}=v^{n}_{i,j+\frac{1}{2},k}+\Delta t\left\{\frac{1}{\rho\Delta y}(p^{n}_{i,j,k}-p^{n}_{i,j+1,k})-\left[\frac{\partial vu}{\partial x}\right]^{n}_{i,j+\frac{1}{2},k}-\left[\frac{\partial v^2}{\partial y}\right]^{n}_{i,j+\frac{1}{2},k}-\left[\frac{\partial vw}{\partial z}\right]^{n}_{i,j+\frac{1}{2},k}\right\} \tag{7}$$

$$w^{n+1}_{i,j,k+\frac{1}{2}}=w^{n}_{i,j,k+\frac{1}{2}}+\Delta t\left\{\frac{1}{\rho\Delta z}(p^{n}_{i,j,k}-p^{n}_{i,j,k+1})+g-\left[\frac{\partial wu}{\partial x}\right]^{n}_{i,j,k+\frac{1}{2}}-\left[\frac{\partial wv}{\partial y}\right]^{n}_{i,j,k+\frac{1}{2}}-\left[\frac{\partial w^2}{\partial z}\right]^{n}_{i,j,k+\frac{1}{2}}\right\} \tag{8}$$

where, the square brackets represent the first order finite difference approximations of the terms inside them. The donor cell differencing method is used for the advective terms of the equations of motion in the first order computation and the procedure of second order approximation is discussed in the next section.

2.3 Numerical algorithm

In the numerical computation procedure the equations are solved by means of a time marching method. The solution process starts with a given set of initial conditions and the variables u, v, w and p are computed iteratively to satisfy the boundary conditions at each time step. In the first order computation, the velocity components u^{n+1}, v^{n+1} and w^{n+1} at time level $n+1$ are estimated for all cells in the fluid domain from equations (6), (7) and (8) using full upstream (donor cell) difference expressions for the advective terms. However, u^{n+1}, v^{n+1} and w^{n+1} obtained from these equations do not necessarily satisfy the continuity equation. Then the iterative adjustment of the pressure in each cell is done to satisfy the continuity equation at time level $n+1$.

Obtaining better resolutions for some problems sometime becomes difficult with simple first order finite difference approximations. In order to increase the accuracy of the computation we, therefore, have introduced second order finite difference approximations in the present simulation for velocity components and the surface elevation function. The procedure of the second order computation varies slightly from the general first order algorithm described above. Following the modified MacCormack method[6] the sequence of this computation can be described as follows:

First, an estimate for F^{n+1} is computed using first order accurate full upstream approximation and the result is called as $\tilde{F}$. The expression can be written as

$$\tilde{F}=F^n+\Delta t\{f^n_{upstream}\} \quad (9)$$

where, f denotes the terms included in the curly brackets ({ }) of the equations (6), (7), (8) and F designates the variables u, v, w etc. Next, $\tilde{\tilde{F}}$ is computed from the same expression (Eq. 9) considering full downstream approximation, but using $\tilde{F}$ values in place of F^n, i, e,

$$\tilde{\tilde{F}}=\tilde{F}+\Delta t\{f^{n+1}_{downstream}\} \quad (10)$$

Then the second order accurate value for F^{n+1} is given by the average of F^n and $\tilde{\tilde{F}}$ as

$$F^{n+1}=\frac{1}{2}(F^n+\tilde{\tilde{F}})$$

$$=F^n+\frac{1}{2}\Delta t[f^n_{upstream}+f^{n+1}_{downstream}] \quad (11)$$

This procedure is used not only for u, v, w calculations but also for the calculation of free surface elevation.

3. Boundary Conditions

The three dimensional wave tank used in this study is shown in Fig. 2. L_E is the length of the effective or working zone of the tank and L_R is the length of velocity reduction zone. Six boundaries of the tank are treated applying the following conditions.

3.1 Wave generating condition

The left end of the tank ($S1\equiv$AEHD) is considered as the wave generating end and the equations used for wave generation are:

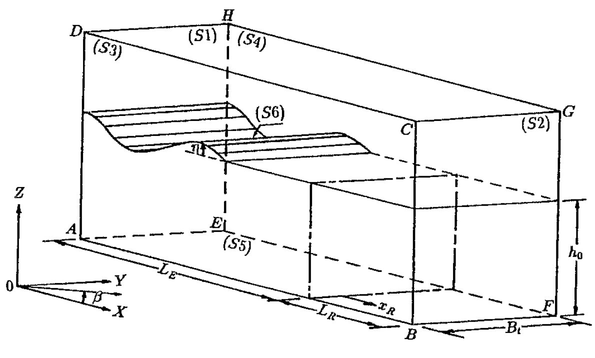

Fig. 2 Definition sketch of the 3D numerical wave tank

Velocity components,

$$u=a\omega\cos\beta\frac{\cosh(kz)}{\sinh(kh_0)}\sin(kx\cos\beta+ky\sin\beta-\omega t) \quad (12)$$

$$v=a\omega\sin\beta\frac{\cosh(kz)}{\sinh(kh_0)}\sin(kx\cos\beta+ky\sin\beta-\omega t) \quad (13)$$

$$w=-a\omega\frac{\sinh(kz)}{\sinh(kh_0)}\cos(kx\cos\beta+ky\sin\beta-\omega t) \quad (14)$$

and the free surface elevation,

$$\eta=a\sin(kx\cos\beta+ky\sin\beta-\omega t) \quad (15)$$

where,

a : amplitude of the wave,
ω : angular frequency,
k : wave number,
h_0 : still water depth,
β : wave propagation angle, measured from x-axis on x-y plane.

As η is measured from still water level, the free surface height h, therefore, becomes

$$h=h_0+\eta \quad (16)$$

where h is measured from the bottom of the tank.

3.2 Open boundary condition

The right end of the tank ($S2\equiv$BFGC, Fig. 2) is considered as the open boundary. A zone (L_R) adjacent to this end is used for the reduction of vertical velocity w exponentially by

$$w_r=w\cdot\exp(-\alpha x_R/L_R) \quad (17)$$

where, α is a nondimensional constant. w is calculated from the governing equations and then it is multiplied by the above exponential function to reduce the amplitude of the wave. Thus the reduced velocity w_r inside VRZ is obtained.

After the reduction of vertical velocity, Sommerfeld radiation condition

$$\frac{\partial\phi}{\partial t}+c\frac{\partial\phi}{\partial x}=0 \quad (18)$$

is applied at the right end of the tank. Where, ϕ is any variable and c is the phase velocity or celerity of the waves given by

$$c=\sqrt{\frac{g\lambda}{2\pi}\tanh(2\pi h_0/\lambda)}\Big/\cos\beta \quad (19)$$

where, λ is wave length. The finite difference approximation of Eq. 18 used here is

$$\frac{\phi^{n+1}(IM)-\phi^n(IM)}{\Delta t}+c\frac{\phi^n(IM)-\phi^n(IM-1)}{\Delta x}=0 \quad (20)$$

where, IM represents the boundary point of the finite grid system in x-direction and $IM-1$ is the point just before IM. n is the current time step and $n+1$ is the next one.

3.3 Other boundaries

Lateral boundaries of the tank ($S3\equiv$ABCD and $S4\equiv$

EFGH, Fig. 2) are treated by two different optional methods. One method is the imposition of periodic or cyclic boundary for which the following equations are used.

$$[h, u, v, w, p]_{\text{at } S3} \equiv [h, u, v, w, p]_{\text{at } S4} \tag{21}$$

These conditions are imposed after computing the new velocities using equations (6), (7), (8) and after each pressure iteration.

The other one is free-slip condition where velocities normal to the walls are taken as zero and tangential velocities have no normal gradients. In mathematical form, these conditions can be written as,

$$v=0 \tag{22}$$

$$\frac{\partial u}{\partial y}=0 \tag{23}$$

$$\frac{\partial w}{\partial y}=0 \tag{24}$$

Bottom of the tank ($S5 \equiv$ ABFE) is also treated as a free-slip rigid wall and the conditions used there are,

$$w=0 \tag{25}$$

$$\frac{\partial u}{\partial z}=0 \tag{26}$$

$$\frac{\partial v}{\partial z}=0 \tag{27}$$

3.4 Free surface condition

The location of the free surface is evaluated by using free surface elevation function $\eta(x, y, t)$, whose value is updated in every time step of calculation for each cell by the free surface kinematic condition

$$\frac{\partial \eta}{\partial t}+u\frac{\partial \eta}{\partial x}+v\frac{\partial \eta}{\partial y}=w \tag{28}$$

The atmospheric pressure is set at the free surface.

4. Assessment Techniques

Two assessment techniques, which were used in our previous paper[5] are also used here for the evaluation of the performance of the numerical tank. Those are as follows:

4.1 Computation of energy

Kinetic energy in a fluid region is calculated from

$$E_k=\rho\int_{x_1}^{x_2}\int_{y_1}^{y_2}\int_{0}^{h}\left[\frac{1}{2}(u^2+v^2+w^2)\right]dzdydx \tag{29}$$

inside the effective zone of the tank. Where, x_1, x_2 are two planes parallel to y-axis and y_1, y_2 are two planes parallel to x-axis. Here the distance between y_1 and y_2 is taken as the width of the tank (B_t, Fig. 2) and kinetic energy is calculated within one wave length span in x-direction.

4.2 Repeatability of wave profile

In this scheme the wave profiles are plotted at different positions inside the effective zone of the tank and compared with each other. For regular waves the wave profiles should repeat any where in the tank except inside the velocity reduction zone. If the profiles appear identically we can understand that the computational domain is free from disturbance.

5. Results of the Computation

Before discussing the results of the numerical wave generation of this study, it is necessary to discuss about the optimization of the parameters used in the velocity reduction technique. After several numerical experiments and parameter studies in our two dimensional computation[5] we have already found out the optimum ranges of α and the length of velocity reduction zone for expected performance of the open boundary. We defined the parameter K_R as the ratio of the length of VRZ to wave length. Choosing a suitable set of these parameters from that results (e.g., $K_R=4$, $\alpha=0.15$ etc.), we have applied them in the present computation.

5.1 Comparison of the generated waves

We have used both first and second order finite difference approximations in the simulation of this study to generate waves numerically. Table 1 shows the conditions of the computations for different mesh sizes. Three mesh sizes are used for both first and second order computations having $12\Delta x$, $24\Delta x$ and $48\Delta x$ per wave length. Time increments and wave parameters (i.e, wave height H_W, wave period T etc.) were kept constant for all the cases with $\beta=0$. Wave profiles are plotted for three different positions inside the effective zone of the tank. First point is taken one wave length apart from the wave generating end. Second one is 3λ apart from the first and the third one is also 3λ apart form the second. Fig. 3 shows the comparison of the waves produced by using rather coarse meshes ($\lambda/\Delta x=12$). Utilization of the full upstream (donor cell) differencing method in first order computation creates severe numerical damping as shown in Fig. 3(a). In this case, wave amplitude decreases gradually as it proceeds forward. It is also clear from this figure that, the crests and troughs of the third wave (chain line, $x=7\lambda$) are shifted right side. It means that, not only the characteristics of the waves change rapidly but numerical phase error also occurs in this case.

Fig. 3(b) is for the same conditions as in Fig. 3(a) but second order approximations are used here.

Table 1 Conditions of the computations

Method	$\lambda/\Delta x$	Δt (sec.)
First Order (Donor cell differencing)	12	0.0125
	24	0.0125
	48	0.0125
Second Order (Modified MacCormack)	12	0.0125
	24	0.0125
	48	0.0125

Remarkable improvement of the results can be seen in this figure. Wave profiles of the three positions are almost the same, which means that the severe numerical damping in the case of Fig. 3(a) is not occurring here. But this computation is not also free from numerical phase error (it will be more clear if we compare Fig. 3

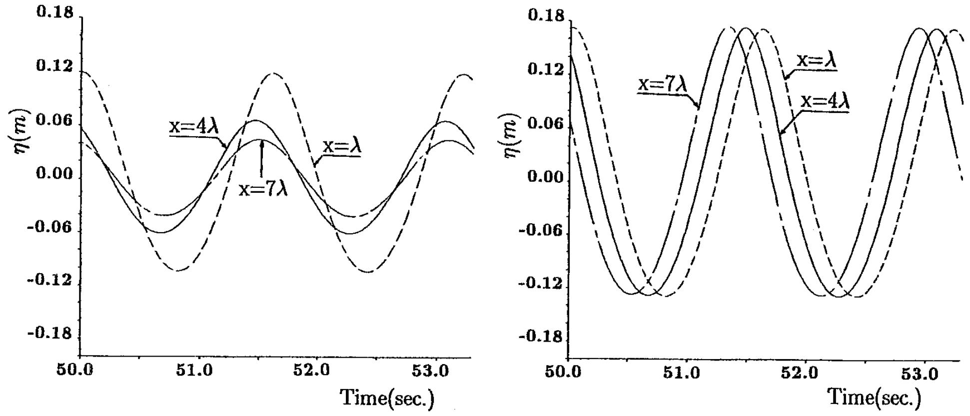

(a) First order (donor cell differencing) (b) Second order (modified MacCormack)

Fig. 3 Time histories of surface elevations at three different positions inside the effective zone of the tank (h_0=2.0 m, T=1.603 sec., H_W=0.27 m, $\lambda/\Delta x$=12)

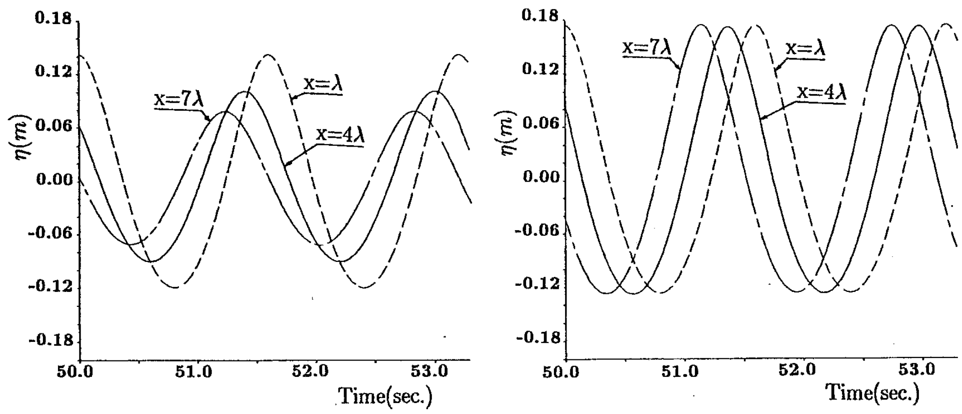

(a) First order (donor cell differencing) (b) Second order (modified MacCormack)

Fig. 4 Time histories of surface elevations at three different positions inside the effective zone of the tank (h_0=2.0 m, T=1.603 sec., H_W=0.27 m, $\lambda/\Delta x$=24)

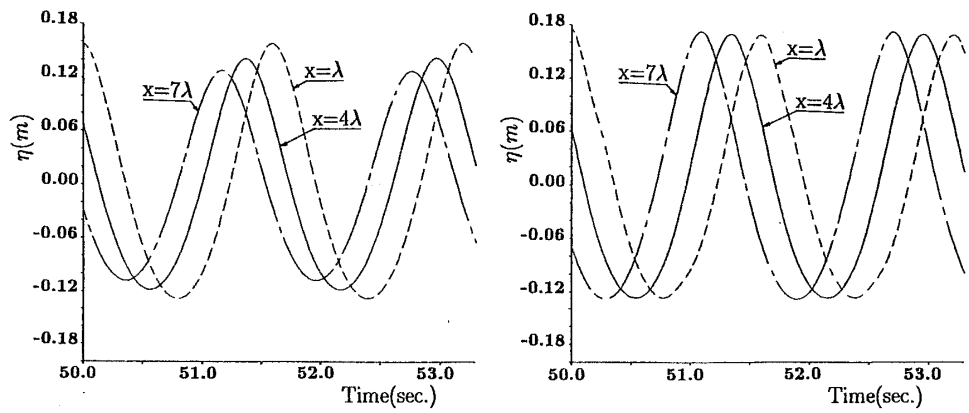

(a) First order (donor cell differencing) (b) Second order (modified MacCormack)

Fig. 5 Time histories of surface elevations at three different positions inside the effective zone of the tank (h_0=2.0 m, T=1.603 sec., H_W=0.27 m, $\lambda/\Delta x$=48)

(b) with Fig. 4(b)).

Fig. 4 is the comparison for $\lambda/\Delta x=24$. Although the results of first order computation (Fig. 4(a)) are slightly improved compared to that of Fig. 3(a), the numerical damping is still strong and the waves are deformed with the advancement of time. On the other hand, satisfactory results are obtained for the same cell size but using second order approximations. As the numerical damping is negligibly small here, the wave profiles are almost identical in this case (Fig. 4(b)).

Results of the third case of computation, i, e, $\lambda/\Delta x=48$, are shown in Fig. 5. Use of finer meshes improves the results noticeably in the first order computation, but the numerical damping is still out of acceptable range (Fig. 5(a)). The results of the second order computation of this case (Fig. 5(b)) are almost similar to that of Fig. 4(b).

If we compare the Figures 3(a), 4(a) and 5(a), it will be clear that, results can be improved up to a certain extent with more finer meshes using first order full upstream (donor cell) approximations, but the results will not be reliable in any case. On the other hand, comparing the Figures 3(b), 4(b) and 5(b), we can easily understand that the second order approximations can give satisfactory results with sufficient accuracy. Of course finer meshes can improve the results in this case also, but $\lambda/\Delta x=24$ may be a suitable choice for practical use.

Fig. 6 shows one typical generation of two dimensional waves propagating at zero angle with x-axis for wave steepness $H_w/\lambda=1/15$ with $S3$ and $S4$ as free-slip boundaries. For $\beta=0$, $S3$ and $S4$ are tested with periodic option and similar results are obtained as for free-slip conditions. That means, for axial propagation of waves lateral boundaries are independent of the conditions, free-slip or periodic. But for oblique waves (i, e, $0<\beta<90°$), these boundaries have important influence on the tank performance. For this case, lateral boundaries must have to be set as periodic ones maintaining the relation

$$B_t=\frac{m\lambda}{\sin\beta} \quad (m=1, 2, 3, \cdots) \tag{30}$$

among the tank width, wave length and wave propagation angle. Then two dimensional oblique waves can also be generated in this numerical wave tank.

Inconsistency of the periodicity of the lateral boundaries may occur for the first wave, when it reaches to these boundaries ($S3$, $S4$) obliquely with maximum amplitude. A linear time increment of the amplitude is imposed to avoid this problem. Thus, after the passing of smaller waves first, when the system becomes steady, the lateral boundaries can perform well as periodic ones. Fig. 7 shows an instant of such kind of wave generation with $\beta=30°$ and $H_w/\lambda=1/15$. From this figure we can see that waves are coming from the corner AD (Fig. 2) of the tank at an angle $\beta=30°$ with x-axis and propagating obliquely through the tank. Waves are coming at the lateral boundaries ($S3$, $S4$) and gradually proceeding forward. $S3$ and $S4$ are repeating the phenomena of each other periodically. This kind of oblique waves may be useful particularly for the model test when the ship model proceeds through

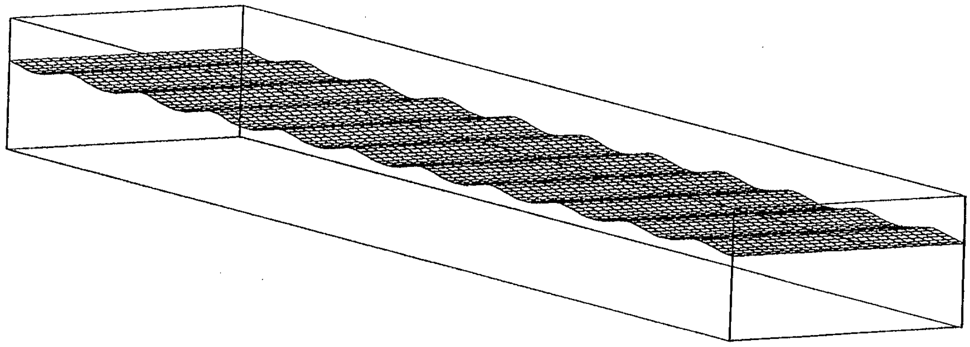

Fig. 6 Waves, propagating along longitudinal axis of the tank ($H_w/\lambda=1/15$, $\beta=0°$)

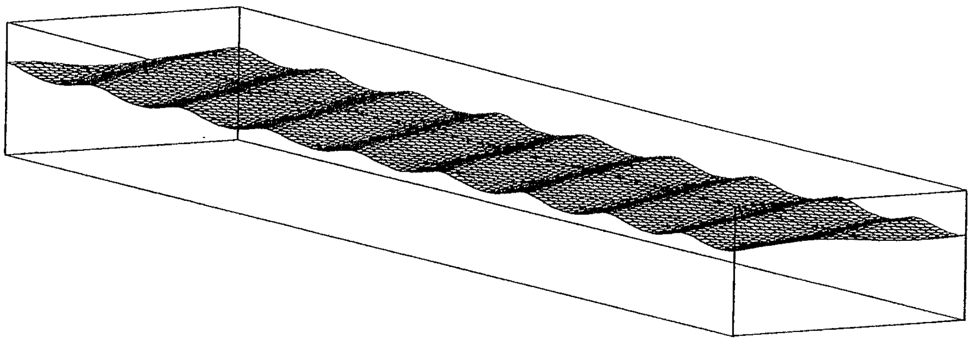

Fig. 7 A typical instant of oblique wave generation ($H_w/\lambda=1/15$, $\beta=30°$)

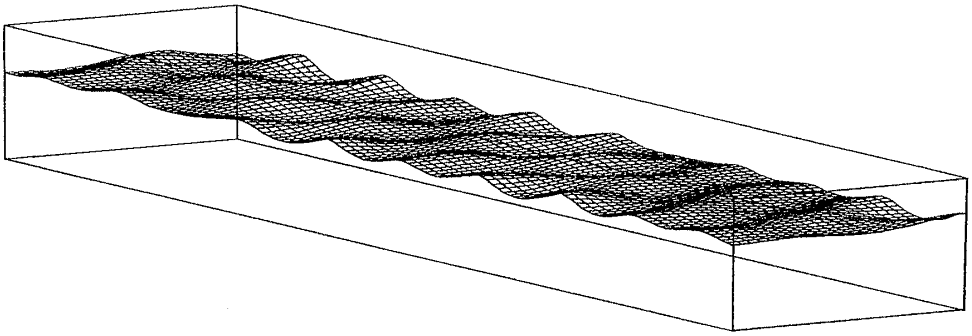

Fig. 8 An example of 3D waves, generated by continuous reflections from the lateral boundaries

oblique waves and the waves hit the model at the angle β. This experiment can easily be performed in the numerical tank even if the tank dimensions are small.

For the generation of three dimensional waves, lateral boundaries are treated by free-slip option and allowed to reflect the waves coming obliquely to them. The first wave approaches the far lateral boundary of the tank ($S4$) and reflects from there and then the reflected wave approaches the other lateral boundary ($S3$) from where it reflects again. Thus, the continuous reflections of the waves from two lateral boundaries create the superimposition of waves which produces three dimensional waves. A typical example of this kind of wave generation is shown in Fig. 8.

6. Conclusion

Using first and second order finite difference approximations in the computations, waves are generated numerically in this study. Three sizes of meshes are used in the computations to see the effect of the fineness of the grids on the numerical simulations. It is seen that coarser meshes create severe numerical damping and the waves deform rapidly when first order full upstream (donor cell) approximations are used in the computation. The superiority of second order computation over first order method is clearly shown by comparing the obtained results in this study. In our present system we could generate two dimensional axial (i, e, the direction of wave propagation is parallel to longitudinal axis of the tank) or oblique waves numerically. For oblique wave generation, there is a relation among tank width, wave length and its propagation angle which governs the operation of lateral periodic boundaries. Three dimensional waves could also be generated in this numerical tank by continuous reflections of the waves from the lateral boundaries.

Acknowledgment

The authors would like to express their gratitude to Mr. L. Y. Cheng of our group for his helpful discussions regarding this study.

References

1) She, K., Greated, C. A., Easson, W. J.: Development of a Two-Dimensional Numerical Wave Tank, Proceedings of the Second International Offshore and Polar Engineering Conference, Vol. III (1992),
2) Hinatsu, M.: Numerical Simulation of Unsteady Viscous Nonlinear Waves Using Moving Grid System Fitted on a Free Surface, Journal of the Kansai Society of Naval Architects, Japan, No. 217 (1992).
3) Ohyama, T., Nadaoka, K.: Development of a Numerical Wave Tank in Nonlinear and Irregular Wave Field with Non-Reflecting Boundaries, Proceedings of Japan Society of Civil Engineers, No. 429/11-15 (1991).
4) Park, J. C., Zhu, M., Miyata, H.: On the Accuracy of Numerical Wave Making Techniques, Journal of The Society of Naval Architects of Japan, Vol. 173 (1993).
5) Arai, M., Paul, U. K., Cheng, L. Y., Inoue, Y.: A Technique for Open Boundary Treatment in Numerical Wave Tanks, Journal of The Society of Naval Architects of Japan, Vol. 173 (1993).
6) Hirt, C. W.: Numerical Fluid Dynamics, A Short Course, Flow Science Inc., Los Alamos, N. M., U. S. A. (1982).
7) MacCormack, R. W.: Numerical Solutions of the Interaction of a Shock Wave with a Laminar Boundary Layer, Proceedings of the Second International Conference on Numerical Methods in Fluid Dynamics, Springer-Verlag, Berlin (1970).